33RD CONGRESS
OF THE INTERNATIONAL COUNCIL
OF THE AERONAUTICAL SCIENCES
STOCKHOLM, SWEDEN, 4-9 SEPTEMBER, 2022

ICAS 2022 SWEDEN

Optimization of an Active Damping System for use with a Single Strut Mount

Jennifer Pereira[1]

[1]National Research Council Canada

Abstract

A study was performed to optimize the effectiveness of a two degree-of-freedom active damping system for use with a single strut mount. With the active damping system and its control optimized, vibrations at the first resonance were reduced by 9.5 to 38.1 dB in pitching moment and 11.3 to 35.5 dB in rolling moment. The effectiveness of the damping system resulted in reliable averaged data such that both lateral and longitudinal data obtained on the same model using a three strut mount compared well to the single strut data. With the single strut mount data validated, continuous motion runs were performed at three different rates. The optimal step size and averaging window were found to vary with pitch or yaw rate. Comparing the results using continuous motion versus step-pause motion showed excellent agreement throughout the linear range and resulted in an 80% reduction in run time for pitch sweeps and a 90% reduction in run time for yaw sweeps.

Keywords: active damping, single strut mount

1. Introduction

During wind tunnel tests, models can be mounted to a single strut instead of a traditional three strut support to reduce the interference between the model and the support system. Moreover, the use of this mounting system simplifies strut tare and interference corrections and reduces the amount of wind tunnel time spent on the latter. To further reduce the amount of wind-on time, a continuous pitch/yaw system may be employed, although continuous pitch/yaw measurements require the use of an internal balance in conjunction with the single strut to measure high frequency loads on the model. Previous tests at the National Research Council Canada have been performed with this arrangement but showed excessive vibrations of the model near stall, thus limiting the testing envelope. These large amplitude vibrations resulted in increased uncertainty in the measurements over the range of incidence investigated. Beyond this, the more concerning effect involves overstressing the internal balance. As such, reducing the amplitude of these vibrations has been a longstanding objective.

Damping of sting-mounted and strut-mounted aircraft models has been attempted over the years and several devices and methods have been proposed. Passive devices have been investigated with limited success [1] [2] [3]; however, these only work for a particular model and configuration, thus making them impractical during production tests. Active damping systems have been attempted with various degrees of success on aft sting-mounted models [4] [5]. However, an active damping system for a belly strut-mounted model (illustrated in Figure 1) has not been developed extensively. Previous work [6] has indicated that the dominant source of vibrations in this mounting arrangement is the flexures from the internal balance (particularly in the pitching and rolling moment directions) rather than the strut itself. As such, the most promising solution is a displacement cancellation device placed between the model and balance that would prevent the balance modes from being excited by external vibrations felt by the model. A prototype of such a system was successfully developed, but showed shortcomings due to saturation of its damping in post-stall. As such, the objective of the current study was to optimize the damping system to reduce the large amplitude vibrations of the model to an acceptable threshold over a wide range of incidence angles.

Figure 1 - Single strut mounting configuration.

2. Active Damping System

The active damping system (ADS) was designed to fit entirely within the fuselage of the model. The main components of the ADS are shown in Figure 2. The main strut was attached to the taper block, which held the ground side of the internal balance. The live side of the balance then fit into a separate balance block. The piezoelectric actuators, which counteracted the vibration of the balance, were attached to the balance block via tie rod ends containing spherical bearings. At the back, a pin, equipped with a spherical bearing, was used as a pivot, and four flexures were placed between the model and balance block to avoid any shear forces acting on the actuators. To prevent tensile loading on the actuators, a compression spring was mounted in parallel with the actuators. Due to the precision required in manufacturing these pieces, the actuators were connected to the spring bracket by a pair of custom made spherical setscrews.

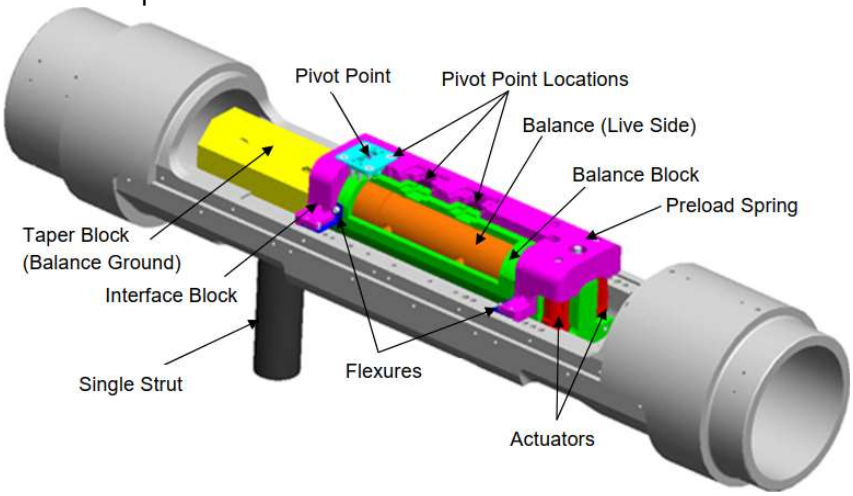

Figure 2 - Active damping system.

In the original design, the pivot point was fixed, and the resulting moment arm was too long for pitching moment control. As a result, in post-stall (where vibration amplitudes are highest), the actuators became saturated, leaving little range for rolling moment control. As a compromise, the damping system was tuned to provide more damping in rolling moment at the expense of pitching moment control. However, since the required restoring force for the actuators increases with a reduction in moment arm, it was possible that the actuators become saturated for small moment arms due to the large restoring forces required. This suggests that there is an optimal pivot point, and as such the new design incorporated three possible pivot point locations to determine which would allow optimal pitching and rolling moment control. The original design included a pivot point location denoted as aft in Table 1. Two new pivot points, denoted as central and fore, had smaller pitching moment arms than the original design.

Table 1 - Pivot point locations available on the ADS

Location	Aft	Central	Fore
Axial Distance from Actuators (inches)	11.65	8.90	6.15

The active damping system used the internal balance output as the control variable and employed a proportional-integral-derivative (PID) feedback controller to apply active control. The controller itself was written in the LabView Real-Time platform. To maintain a two degree-of-freedom control system (for pitching moment and rolling moment control) and maximize the efficiencies of the actuators, the pair of actuators was arranged as described in Figure 3. During pitching moment control, the actuators deflected in phase, thus sharing the required load. In rolling moment control, the actuators worked out of phase, once again sharing the required load. The controller was programmed to provide the correct displacement for each actuator. This involved converting the disturbance displacements into required actuator input voltages (one to counteract pitching moment disturbances and one to counteract rolling moment disturbances). Each required voltage input was sent through its own PID loop. The required PID voltages were then added/subtracted according to Figure 3 for each actuator.

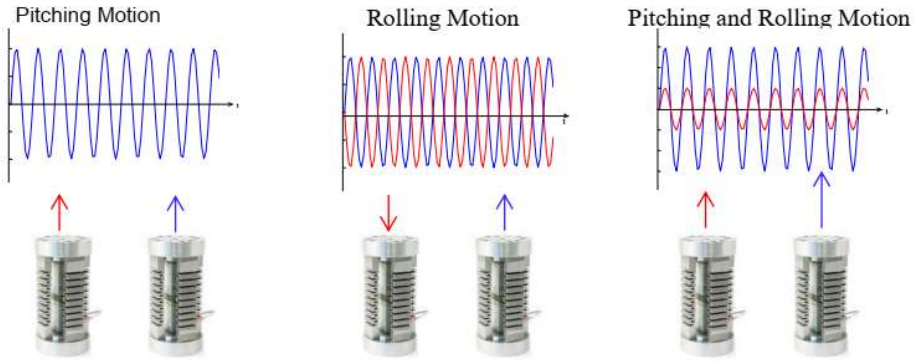

Figure 3 - Actuator control arrangement.

3. Wind-Off Results

To test out the impact of the pivot points as well as the effectiveness of the damping system, a generic aircraft model was set up outside of the wind tunnel in a configuration representing cruise conditions. The model was first tuned at the aft pivot point on the ADS.

For tuning, a Matlab Simulink model was used to predict the behavior of the system and the required constants for the PID control. As the pitching moment and rolling moment control were largely uncoupled, the Simulink model consisted of two single degree-of-freedom systems, each represented by Figure 4. The response of the system to a disturbance from the actuators is represented by the plant, G. In practice, the transfer function representing the plant was obtained by applying a chirp from the actuators and measuring the response of the system from the balance. In doing so, conversion from the voltage applied to the actuators to the corresponding displacement of the balance was obtained. The response of the balance and the system to an outside disturbance, such as an impulse, was represented by the function, F. This essentially provided the open-loop transfer function from the input (r) to the output (y) without any feedback. The sensor dynamics block, H, converted balance displacement to equivalent voltage input to the actuators. Finally, the PID controller was represented by the block C. The transfer functions F and G were both continuous systems (functions of s), whereas the balance measurements and controller both required the use of an A/D board and were discrete systems (function of z).

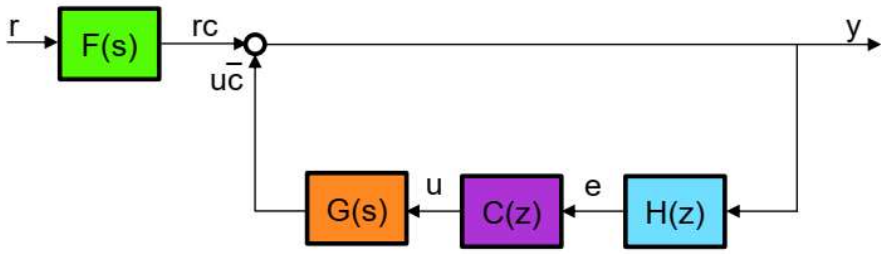

Figure 4 - Simulink feedback control system architecture.

To improve the accuracy of the Simulink model, the transfer functions F and G were obtained from actual measurements on the aircraft model and represented by polynomial transfer functions. The simulation was then run by varying the PID constants until optimal damping was obtained.

Since the pitching and rolling moment responses were expected to be uncoupled, the transfer functions F and G were obtained first in pitching moment excitation only and then in rolling moment excitation only. The magnitude of the frequency responses are shown in Figure 5. The results indicate that in the pitching moment direction, a first resonance occurred at 13.7 Hz. A resonance at 7 Hz corresponded to a strut mode, which could not be damped out by the ADS. Similarly, the frequency responses in the rolling moment direction indicated a first resonance at 10.4 Hz, a second resonance at 48.8 Hz and a minor peak at 8.2 Hz. Further investigation proved that the peak at 8.2 Hz corresponded to a strut mode, which could not be damped out by the ADS; thus, this mode was not simulated for control purposes.

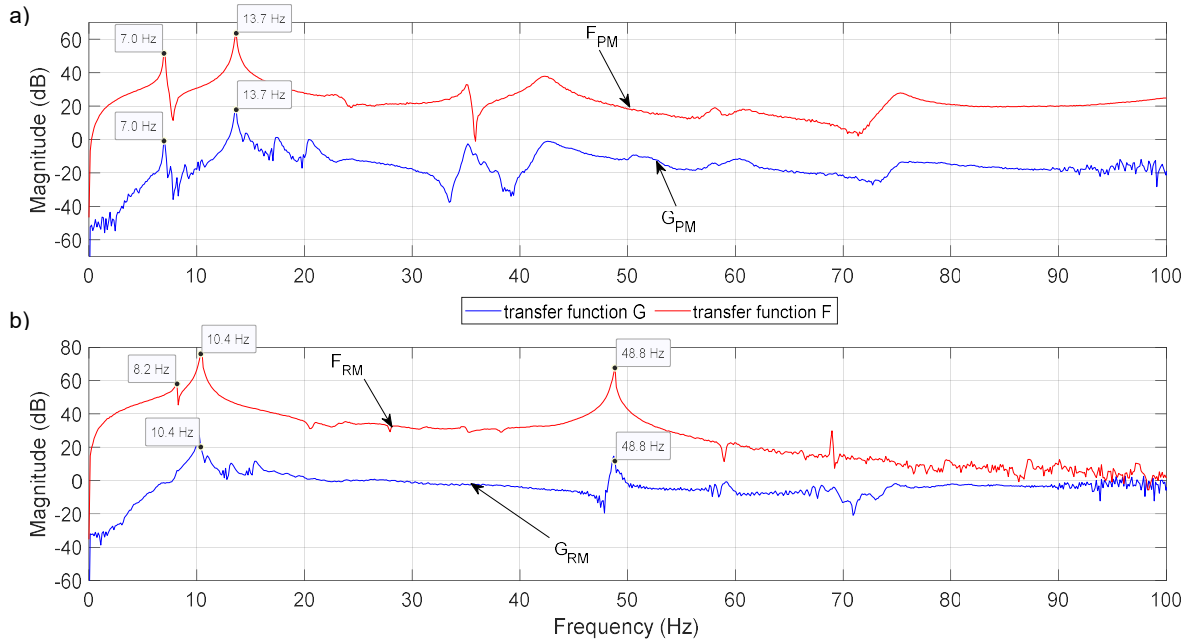

Figure 5 - Magnitude of frequency response functions for a) pitching moment control and b) rolling moment control.

The transfer functions were input into the Simulink model and run to determine the accuracy of the simulation. To determine the optimal PID constants, various values of proportional constant, Kp, integral constant, Ki, and derivative constant, Kd, were attempted, although changes to Kp alone were found to be stable and sufficient. The real system behavior was well-represented by the Simulink model for pitching moment control as shown in Figure 6, with the simulation giving excellent predictions at the optimal Kp_{PM} value of -15. There was good agreement between the simulation and experiment for the rolling moment control for $Kp_{RM} > -2.5$. The reason for this discrepancy was that the strut mode at 8.2 Hz could not be attenuated with the ADS. Furthermore, the two results began

to deviate as at this level of control, the model mode was significantly damped such that the magnitude of the strut mode became the dominant mode in the system response. To avoid this situation, the proportional constant of Kp_{RM} = -2.5 was selected.

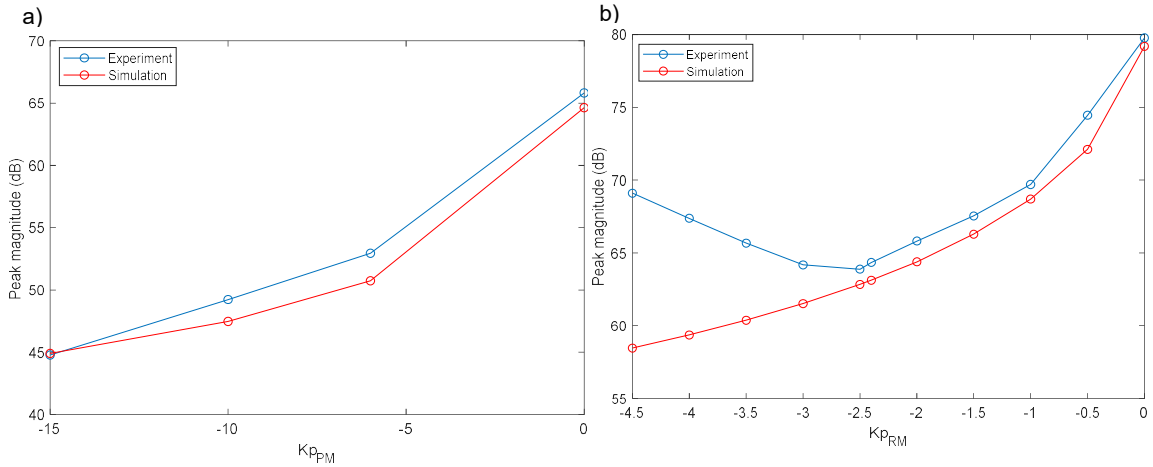

Figure 6 - Comparison of simulated and experimental results on a) pitching moment control and b) rolling moment control.

To verify the proper operation of the damping system during a typical test, a tap test was performed to simultaneously excite the model in the pitching and rolling moment directions. The PID constants of Kp_{PM} = -15 and Kp_{RM} = -2.5 were used. The results in Figure 7 indicate that the two degree-of-freedom PID control did not cause any unwanted coupling between pitching and rolling moment directions. Furthermore, the control resulted in reductions in peak amplitude at the first resonance of 20 dB in pitching moment and 18.5 dB in rolling moment.

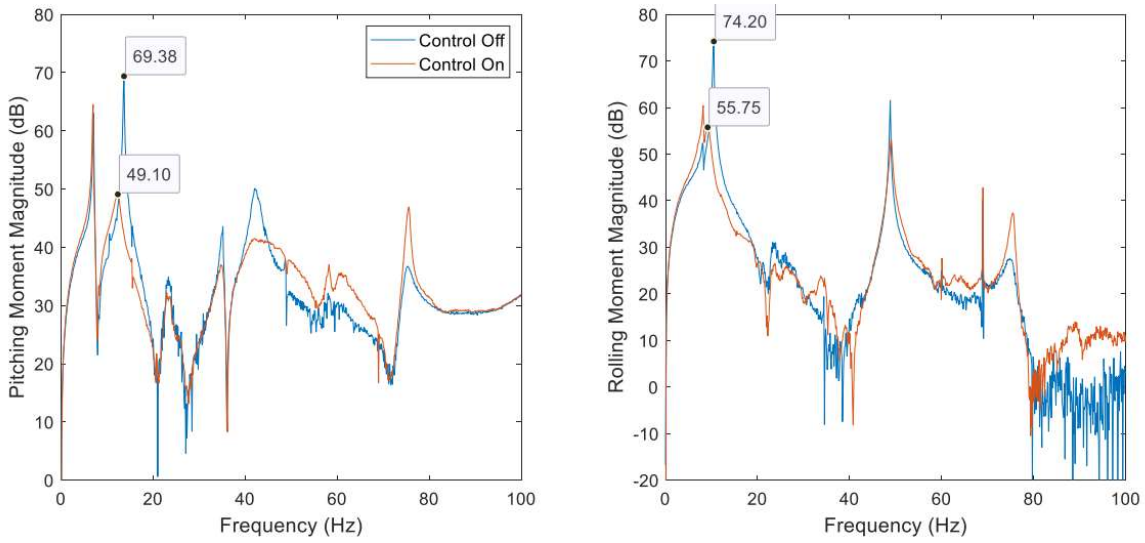

Figure 7 - Effect of control on pitching moment and rolling moment peak magnitudes.

The ADS was then tuned at the two new pivot locations (central and fore) to assess the impact of the pivot point on the bandwidth of the actuators. As the pivot point only affected the moment arm in the axial direction, moving the pivot point only affected the pitching moment results. In fact, the maximum attenuation obtained using any of the pivot points remained the same: approximately 20 dB in pitching moment and 19 dB in rolling moment. However, the introduction of a smaller moment arm increased the amplification of the model due to actuator stimulus. As a result, larger attenuations could be achieved with smaller values of proportional constant, as shown in Figure 8. For example, if a design point of 15 dB of attenuation was prescribed, this could be achieved with Kp_{PM} = -7 using the aft pivot point or with Kp_{PM} = -4.5 using the fore pivot point. Consequently, the fore pivot point resulted in the largest attenuations and was deemed most optimal.

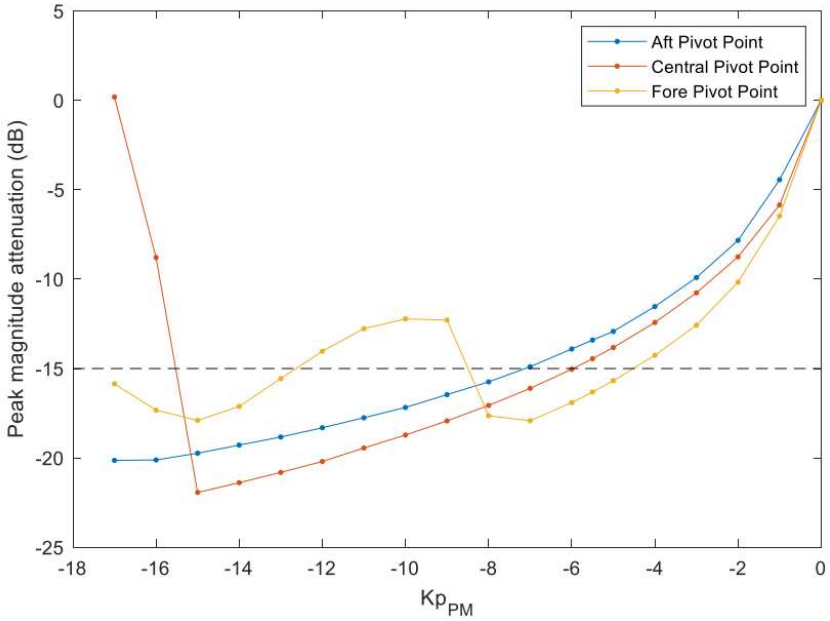

Figure 8 - Effect of pivot point on peak magnitude attenuation at the first resonant frequency.

Taking this into account and comparing to results obtained during wind-on, the largest peak-to-peak amplitudes expected on the balance without damping (which occurred in post-stall) were approximately 17 microns in rolling moment and 3.3 microns in pitching moment. However, it is important to consider that the displacement at the actuators was not the same as the displacement measured by the balance at its flexures. For the pitching moment, normal force flexures of the balance were located ±89 mm away from the balance center. The actuators were placed as close to the balance center as practically possible, but since the balance being used was long compared to the location of its normal flexures, the actuators were in fact placed 188 mm away from the balance center. This constituted an amplification factor of 188/89 = 2.11. Considering the amplification factors accounting for the location of actuators relative to balance flexures, this indicated that in the worst-case scenario, the actuators would require 24 microns of total displacement, but they were limited to 20 microns. As such, the actuators would saturate in post-stall when reaching these maximums. In light of this, a decision had to be made on how to distribute the control to achieve the maximum damping while avoiding the actuators becoming saturated.

One way of choosing these ideal constants is to consider the maximum range of the actuators and ensure that the attenuation remains constant regardless of condition. For example, given that the worst-case scenario required 24 microns of displacement and the actuators were limited to 20 microns, this suggested that the maximum attenuation would be 83%. Therefore, the PID constants were chosen to achieve 83% (~15.5 dB) attenuation. From the results of Figure 6 and Figure 8, this was expected to occur near Kp_{PM} = -6, Ki_{PM} = 0, Kd_{PM} = 0 and Kp_{RM} = -2, Ki_{RM} = 0, Kd_{RM} = 0. These minimum saturation control PID constants were attempted on the aircraft model at the fore pivot point and the results are shown in Figure 9. Peak attenuations at the first resonance of 16 dB in pitching moment and 17 dB in rolling moment were achieved, which slightly exceeded the design goal of 15.5 dB. These results suggested that actuator saturation could be avoided and still offer reasonable peak attenuations that could be consistently achievable throughout the pitch sweep, whether in pre-stall, stall or post-stall.

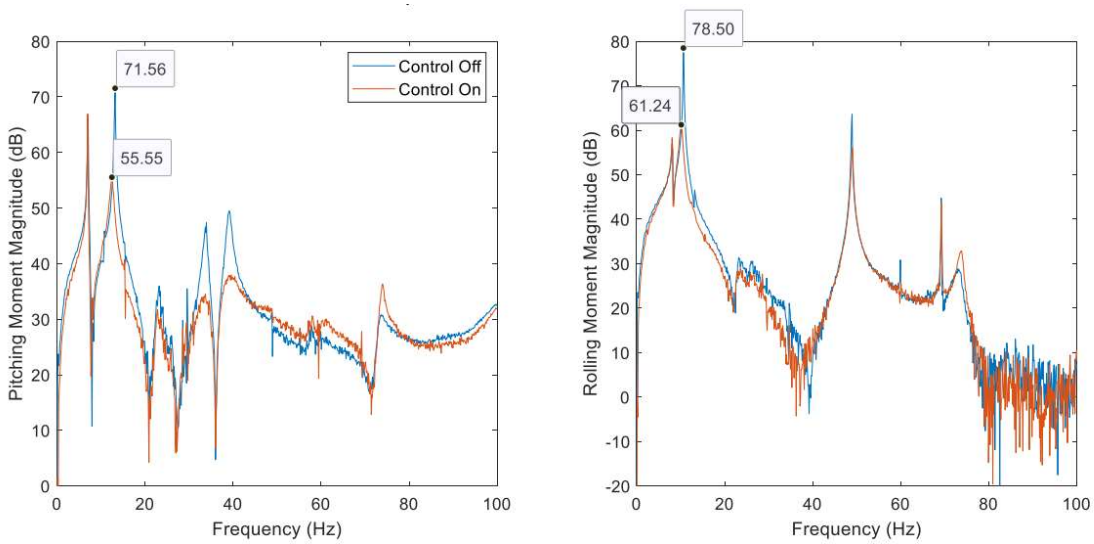

Figure 9 - Effect of minimum saturation control on pitching moment and rolling moment attenuation at the fore pivot point.

4. Wind-On Results

To validate the wind-off results, the setup was then installed in the National Research Council Canada's 2 m × 3 m low-speed wind tunnel. To test the range of expected loads during a typical stability and control test, configurations representing the lower and upper range of these loads were considered. This included two configurations representing the model during cruise and landing conditions. For each configuration, measurements were obtained over a range of model pitch angles (α), and yaw angles (ψ).

While ten different cases were tested, for brevity only three representative cases will be examined in more detail: low vibration for a yaw sweep run, moderate vibration for a pitch sweep at zero yaw angle, and high vibration for a pitch sweep at large yaw angle.

4.1 Low vibration case

The damping system was first tested with the model in the landing configuration undergoing a yaw sweep at α = 8º. This case was not expected to cause large vibrations on the balance. Rather, yaw sweep runs were performed to ensure that the ADS did not cause any unwanted coupling or undesirable behavior during low vibration runs. From the time histories, the standard deviation (σ) of both the pitching moment and rolling moment signals were calculated at each angle in the yaw-pause run. The σ values over the course of the sweep are plotted in Figure 10 and indicate a clear reduction in the vibrations with the use of the ADS. The ADS reduces the standard deviation by 29.8 to 52.5% in pitching moment over the range tested, with a mean value of 41.8%. For rolling moment, the reductions range from 18.8 to 56.3% with a mean value of 36.9%. For both pitching moment and rolling moment, there is no drop in effectiveness with increasing yaw angle indicating that the actuators do not saturate and are able to provide consistent damping throughout the entire yaw sweep.

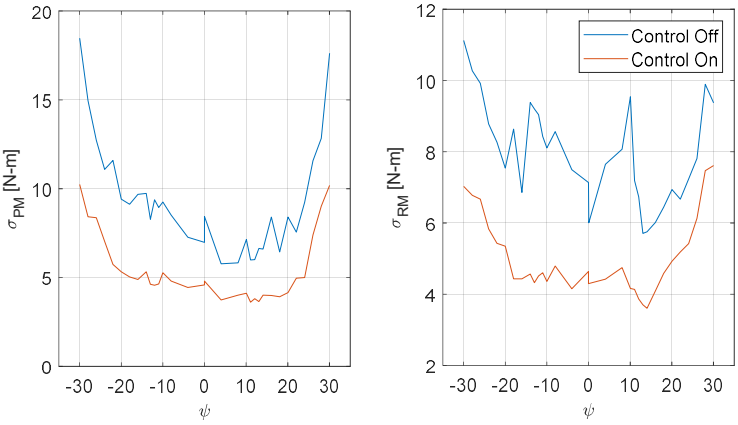

Figure 10 - Effect of ADS on standard deviation of signal during a yaw sweep at α = 8º.

To determine the effect of the ADS from a spectral perspective, fast Fourier transforms (ffts) were performed on the data at three representative points in the sweep corresponding to the linear range (based on yawing moment and rolling moment plots), edge of the linear range and beyond the linear range. The fft results, shown in Figure 11, indicate that peak attenuations at the system's first resonance of 21.8 to 38.1 dB in pitching moment and 22 to 35.5 dB in rolling moment were achieved throughout the angular range tested.

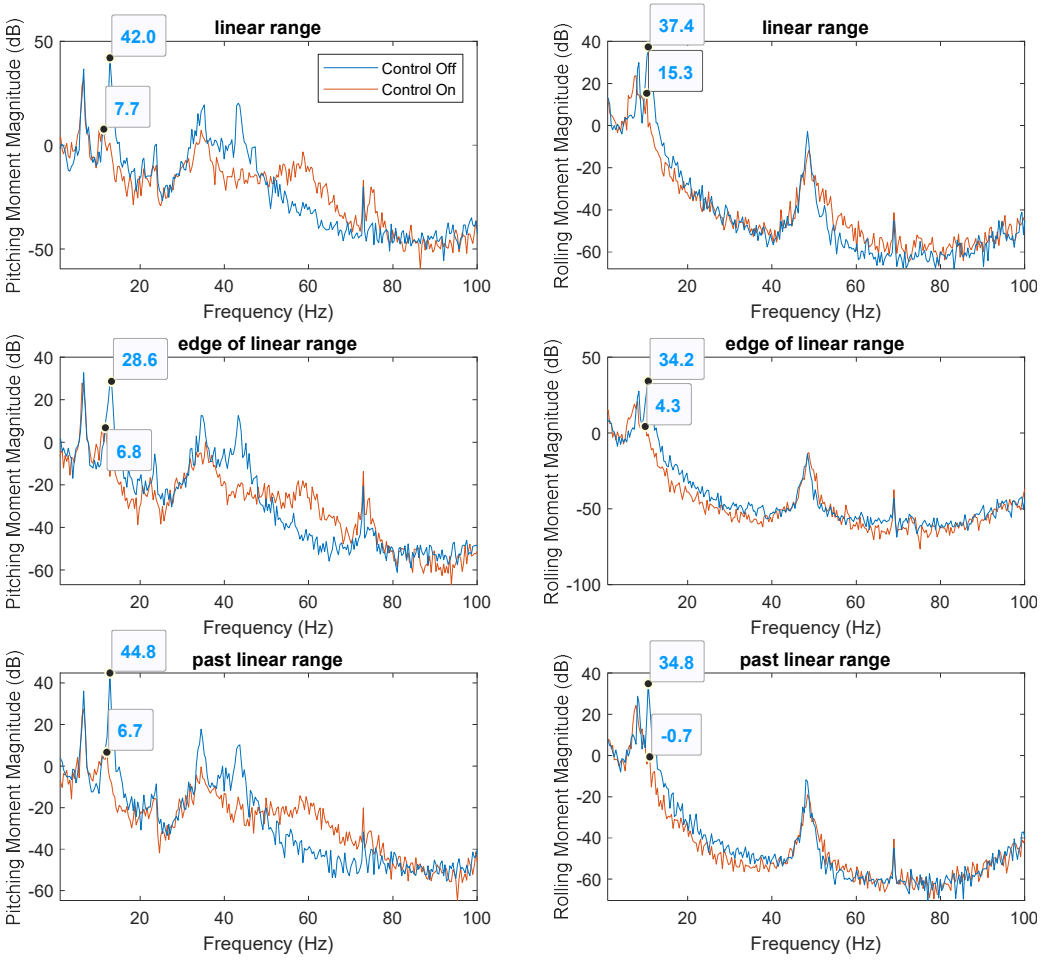

Figure 11 - Effect of ADS on spectral results during a yaw sweep at α = 8º.

4.2 Moderate vibration case

The landing configuration was examined during a pitch sweep with ψ = 0º as this condition was expected to test performance of the damping system for one of the most common types of sweeps performed in typical stability and control tests. To gauge the effectiveness of the ADS, the standard deviation at each step in the step-pause run was calculated for both pitching moment and rolling moment directions. These results, shown in Figure 12, indicate that smaller amplitude vibrations occur with the use of the ADS over the entire pitch sweep. The ADS reduces the standard deviation by 7.8 to 50.2% in pitching moment with a mean value of 31.2%. In rolling moment, the ADS reduces the standard deviation of the vibrations by 13 to 40% with a mean value of 30%.

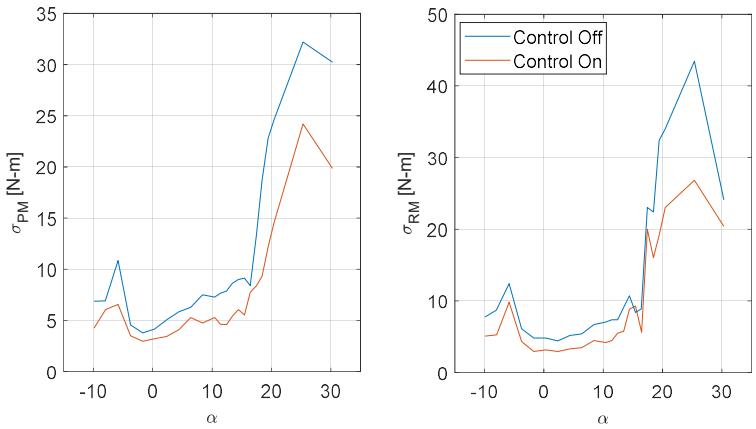

Figure 12 - Effect of ADS on standard deviation of signal during a pitch sweep at ψ = 0º.

To determine the effect of the ADS from a spectral perspective, ffts were performed on the data at three representative points in the sweep corresponding to pre-stall, stall and post-stall. The spectral results, shown in Figure 13, indicate that the ADS was effective in damping out vibrations at the first resonance. This resulted in reductions in peak pitching moment amplitude of 26 dB, 30 dB and 24.1 dB in pre-stall, stall and post-stall regimes. These reductions were higher than the designed 15 dB of reduction, although they were consistent throughout the pitch sweep. Reductions in peak attenuations at the first resonance in rolling moment were found to be 27.1 dB, 24.1 dB and 20.2 dB in pre-stall, at stall and in post-stall regimes. There was a slight dip in the effectiveness of the ADS post-stall, but overall the reductions remained above the design value of 15 dB and remained fairly consistent throughout the pitch sweep.

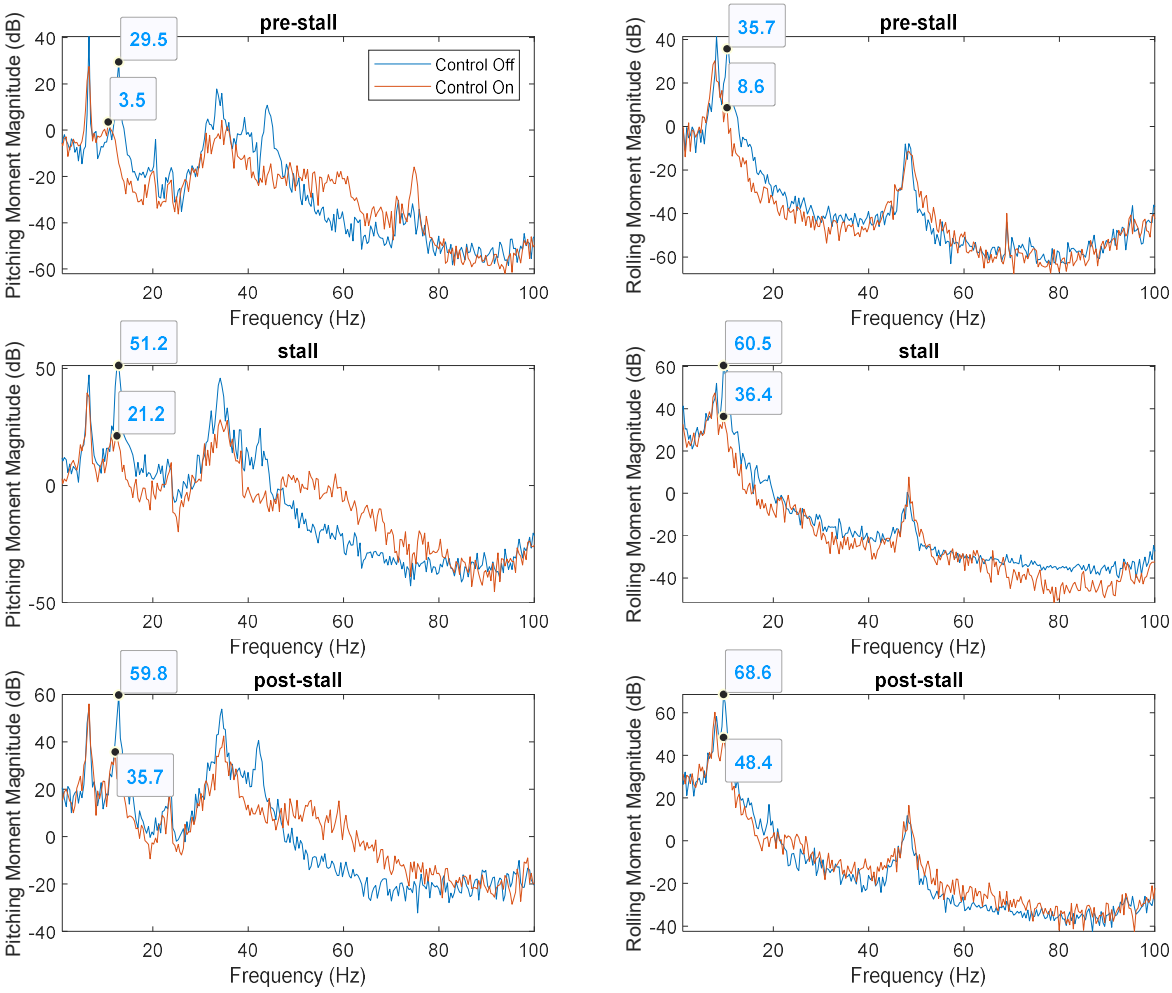

Figure 13 - Effect of ADS on spectral results during a pitch sweep at ψ = 0º.

4.3 High vibration case

Finally, tests were conducted by performing a pitch sweep at ψ = 20º with the model in the cruise configuration. This condition was expected to be among the worst for vibrational purposes and therefore the best test for understanding the capability limits of the ADS. The standard deviation values are plotted in Figure 14 and indicate a reduction in the amplitude of the vibrations with the use of the ADS over the entire pitch sweep. For pitching moment, the attenuations remain fairly consistent with reductions of 17.9 to 45% over the entire angular range and a mean value of 28.5%. For the rolling moment however, the largest attenuations are found at stall and post-stall. These range from 16 to 43% with a mean value of 34.3%. This result is encouraging as the large amplitude vibrations that could harm the internal balance occur after stall and this is where the ADS appears to have the most effect.

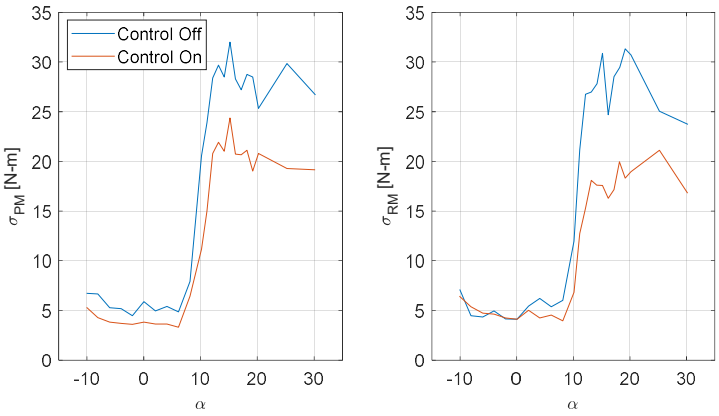

Figure 14 - Effect of ADS on standard deviation of signal during a pitch sweep at ψ = 20º.

The spectral results, shown in Figure 15, indicate 22.2 dB, 17.2 dB and 9.5 dB of peak pitching moment attenuation during pre-stall, stall and post-stall. Similarly, for the rolling moment, at the first peak resonance the attenuation was 23.7 dB, 16.4 dB and 11.3 dB during pre-stall, stall and post-stall. While the post-stall attenuations were below the design value of 15 dB, the ADS was able to maintain the vibrations below the threshold such that the pitching moment and rolling moment signals never exceeded 90% of the internal balance's overall limits. Therefore, even in the worst-case scenario, the ADS was able to achieve its primary goal of avoiding overstress of the internal balance.

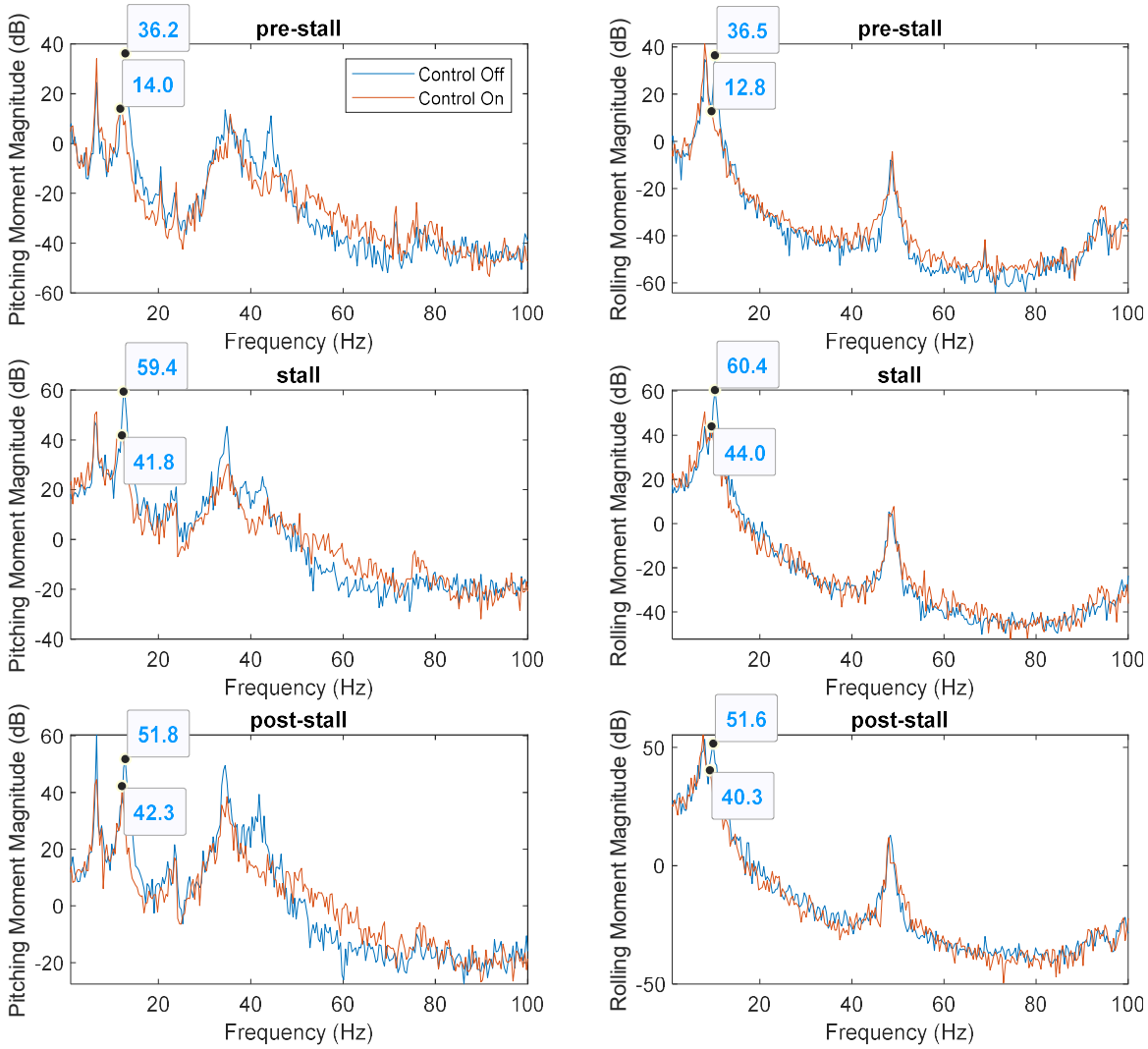

Figure 15 - Effect of ADS on spectral results during a pitch sweep at ψ = 20º.

4.4 Comparison with three strut mount

One of the main objectives of this test was to compare the single strut data to those obtained using a three strut mount. Although the lateral case was not expected to cause large vibrations, the results from the previous section indicated that the ADS had a significant impact in damping out vibrations during the course of a yaw sweep. Therefore, comparison of the lateral coefficients with the three strut mount was performed. Figure 16 indicates excellent agreement between the two for both cruise and landing configurations over the linear range. There is some deviation in the rolling moment outside of the linear range, but this is more representative of the unsteadiness of the flow at these yaw angles. The largest differences between the two for the cruise configuration are 0.028, 0.004 and 0.007 for side force coefficient (C_Y), yawing moment coefficient (C_N), and rolling moment coefficient (C_R). For the landing configuration, the largest differences between the two setups are 0.027, 0.006 and 0.004 for C_Y, C_N and C_R. The close agreement between the two mounting systems indicates that the ADS does not cause any unwanted coupling or undesirable behavior that would contaminate the measurements.

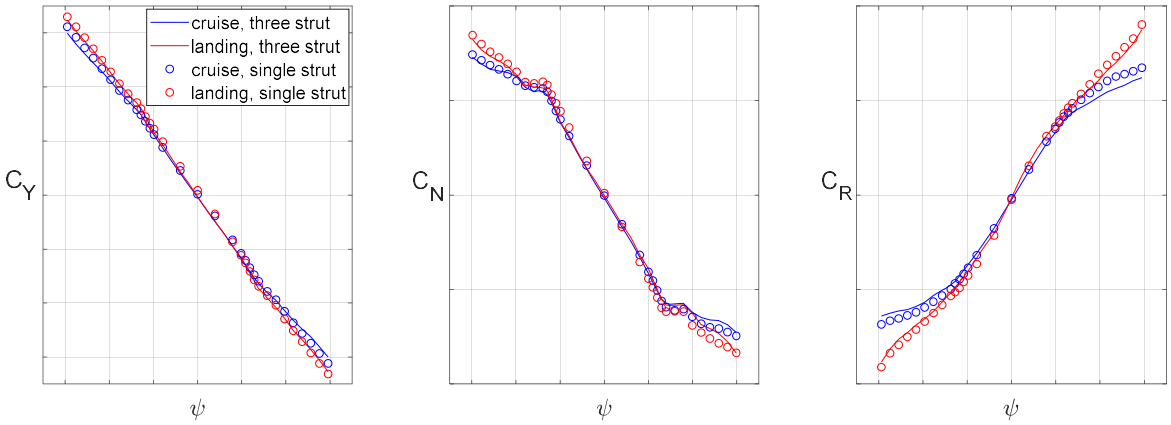

Figure 16 - Comparison of lateral data between three strut and single strut mounts during yaw sweep at α = 8º.

The longitudinal coefficients for both configurations undergoing a pitch sweep at ψ = 0º are shown in Figure 17 and indicate excellent agreement throughout the range tested. There are some minor deviations in pitching moment post-stall, but this is more representative of the uncertainty of the measurements in post-stall. Prior to stall, the largest differences between the two occur with the model in the cruise configuration and are 0.040, 0.045, and 0.0180 for lift coefficient (C_L), pitching moment coefficient (C_M) and drag coefficient (C_D).

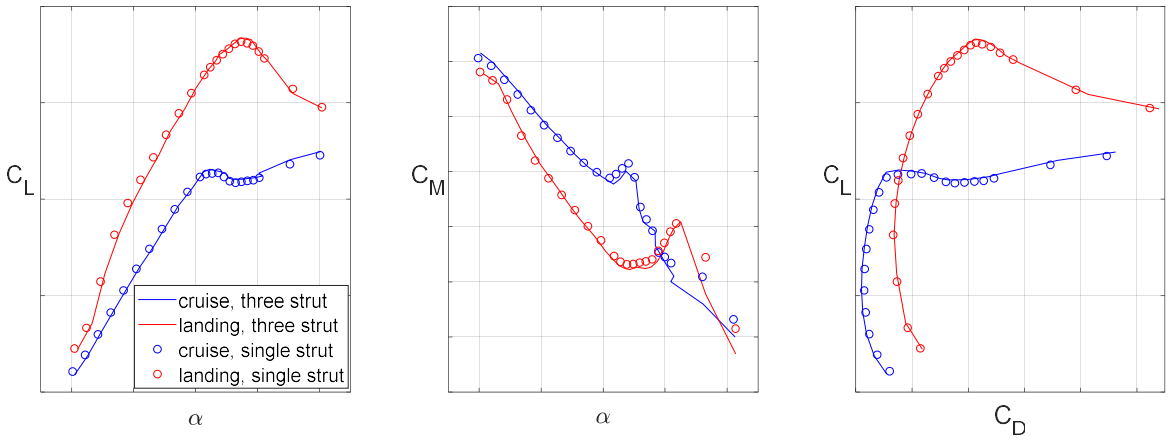

Figure 17 - Comparison of longitudinal data between three strut and single strut mounts during a pitch sweep at ψ = 0º.

4.5 Continuous motion

To validate the results using continuous sweep motion, three rates were examined to ensure quasi-steady flow, equivalent to step-pause motion, while maximizing pitch/yaw rate. The reduced pitch rate (k), is a non-dimensional parameter that governs the flow unsteadiness. It is defined in equation (1) and is a function of the pitch rate ($\dot{\alpha}$), in radians per second, chord (c), and freestream velocity (U_∞).

$$k = \frac{\dot{\alpha} c}{2U_\infty} \tag{1}$$

From McCroskey [7], it is generally understood that for low values of k, the flow should remain quasi-steady and free from unsteady effects associated with dynamic stall (delayed stall, leading edge vortex formation, etc.). For $k < 1 \times 10^{-4}$, unsteady effects are expected to be insignificant [8]. For typical aircraft tests in the 2 m × 3 m tunnel utilizing step-pause motion, the model pitches between steps at a rate of 0.8º/s, which corresponded to $k = 1.7 \times 10^{-5}$ for the test conditions. Consequently, this rate should result in insignificant unsteady effects and was used as the upper limit.

The step-pause map utilized for most pitch sweep runs during the test took 471 seconds to complete. The lower pitch rate was selected to match this run time, thus rendering a pitch rate of 0.087º/s. Another pitch rate was chosen as the midpoint between the lower and upper pitch rates, resulting in a pitch rate of 0.44º/s. A similar exercise was performed for the yaw sweep rates by using the step-pause run time, midpoint and maximum rate. This resulted in the yaw rates shown in Table 2.

Table 2 - Rates tested for continuous motion

Rationale	Pitch Rate (º/s)	Yaw Rate (º/s)
Maximum rate	0.8	1
Pitch rate midpoint	0.44	0.55
Step-motion run time	0.087	0.092

The accuracy of the data averaged from a continuous motion run will depend on both the size of the step interval and the size of the averaging window. Too large of a step interval will result in sparse data points to describe the curve, whereas too small of a step interval would pick up on small oscillations in the curve that are not representative of the true averaged aerodynamic characteristics. Similarly, too small of an averaging window would include an average over a small number of samples, whereas too large of an averaging window would smooth out real variations in the curve. To test out these effects, step intervals ranging from 0.1-0.5º and averaging windows ranging from 0.1-1º were investigated. The errors were calculated as the difference at each point in the sweep compared to the corresponding step-pause run. The mean absolute error for a pitch sweep in the cruise configuration is plotted in Figure 18 as a function of step interval and window size. The results indicate that the window size has a more pronounced effect on the final average or the error in relation to the step-pause run. To minimize the error for this particular pitch rate (0.44º/s), the optimal step interval was 0.4º, whereas the optimal averaging window was 1º.

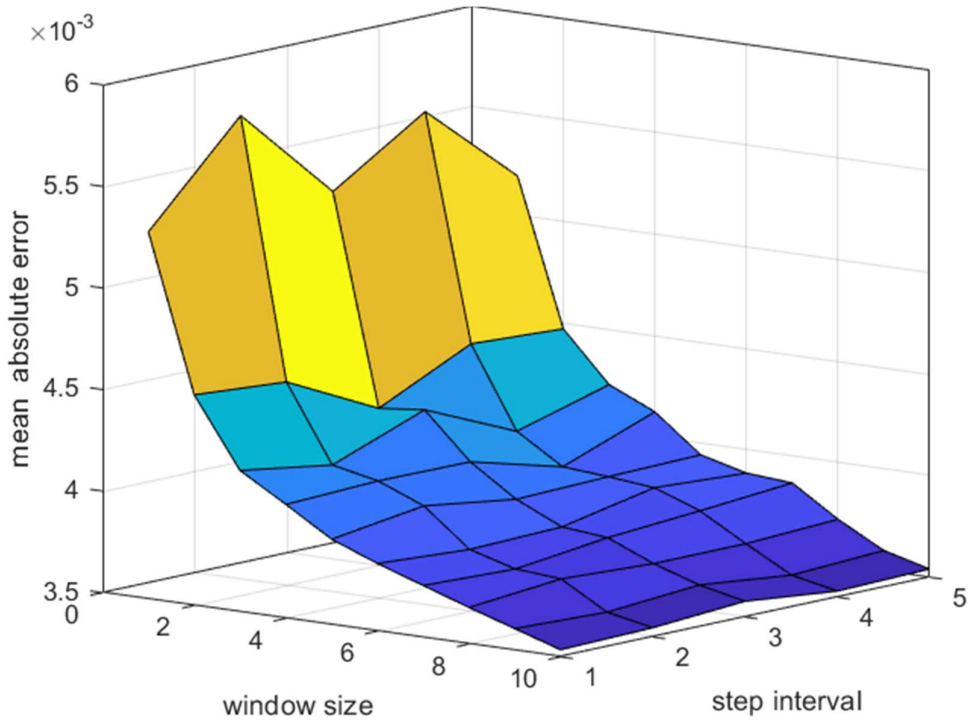

Figure 18 - Effect of step interval and window size on the mean error for a pitch sweep at ψ = 0º.

This same exercise was repeated for all three continuous pitch rates in order to determine the optimal values. For the most part, the optimal window size remained 1º, but the optimal step interval varied. Using the optimal step interval and window size, the results using the three pitch rates are shown in Figure 19 for the cruise configuration. In comparison with the equivalent step-pause run, there is excellent agreement for most of the range. There is some discrepancy right before stall where the continuous motion runs show a slight increase of 0.01 in maximum C_L compared to the step-pause run. Part of this discrepancy may be due to the discretization of points near the maximum C_L in the step-pause run. Therefore, each continuous pitch run was compared to the equivalent step-pause run and the errors calculated. The continuous pitch run with the lowest mean absolute errors was selected as the optimal pitch rate. For both the cruise and landing configurations, the pitch rate of 0.44º/s was chosen as the optimal rate, resulting in an 80% reduction in run time using continuous motion.

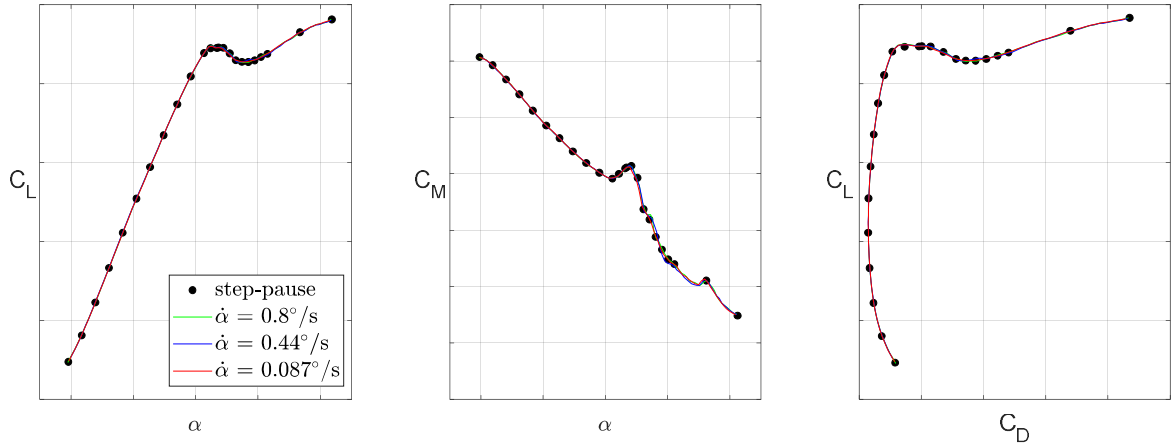

Figure 19 - Effect of pitch rate on longitudinal coefficients for cruise configuration for pitch sweep at ψ = 0º.

The optimal parameters were determined for yaw sweeps as well, with the results shown in Figure 20. Once again, there is excellent agreement between the continuous motion runs and the step-pause run throughout the entire range. The continuous yaw run with the lowest mean absolute errors relative to the step-pause run corresponded to a yaw rate of 1º/s. This rate was selected as the optimal rate which allowed the yaw sweep to be completed in 90% less time.

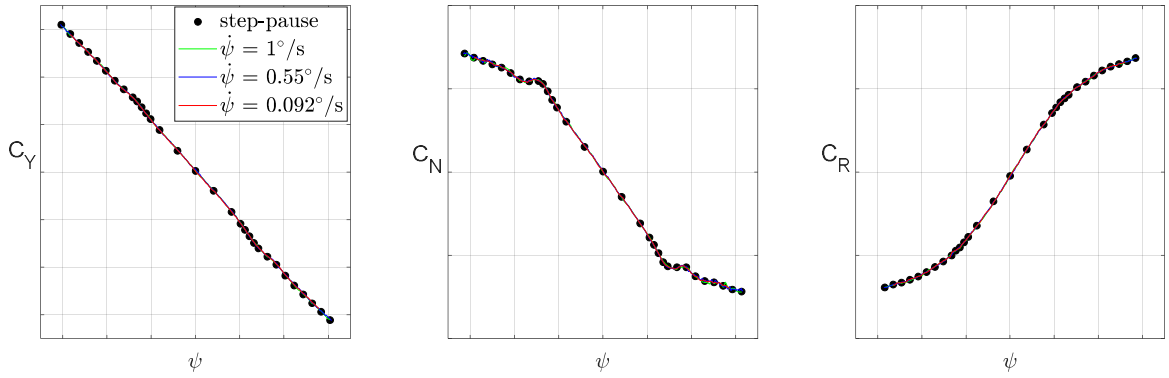

Figure 20 - Effect of yaw rate on lateral coefficients for cruise configuration for yaw sweep at α = 8º.

5. Conclusions

A study was performed to optimize an active damping system for use with a single strut mount. The damping system was modified to allow the pivot point to be moved to achieve optimal pitching moment and rolling moment control. Wind-off tests indicated that moving the pivot point to the foremost position, would provide the largest attenuations and was deemed most optimal.

The wind-off tests also confirmed that the system could be well simulated using a Matlab Simulink model. In order to improve the accuracy of the Simulink model, the transfer functions describing the system's behavior were obtained from actual measurements on the model and represented by polynomial transfer functions. The simulation was then run by varying the PID constants until optimal damping was obtained. Using this method ensured that the optimal constants could be reliably calculated in a short time. The simulation also indicated that during the worst-case scenario, the actuators would become saturated if the control was set to its maximums. To avoid this scenario, the optimal damping was chosen to avoid saturation and set to 83% of its maximum value.

These ideal constants were then used in a wind-on test to validate the results. With the damping system activated, the standard deviations in pitching moment vibrations were reduced by 7.8 to 52.5% and by 13 to 56.3% for rolling moment vibrations. For the worst-case scenario, the damping system was found to be most effective in rolling moment attenuation during post-stall when the risk of overstressing the internal balance is greatest. The damping system was found to be quite effective in damping out vibrations at the first resonance by 9.5 to 38.1 dB in pitching moment and 11.3 to 35.5 dB in rolling moment. The effectiveness of the ADS resulted in reliable averaged data. Consequently, both lateral and longitudinal data obtained on the same model using a three strut mount compared well to the single strut data.

Finally, with the single strut mount data validated, continuous motion runs were performed at three different rates. The optimal step size and averaging window were found to vary with pitch or yaw rate. Using the optimal averaging parameters and comparing the results using continuous motion versus step-pause motion showed excellent agreement throughout the linear range. Using the optimal continuous motion rates resulted in an 80% reduction in run time for pitch sweeps and a 90% reduction in run time for yaw sweeps.

6. Contact Author Email Address

jennifer.pereira@nrc-cnrc.gc.ca

7. Statement

References

[1] Capone F and Igoe W. Reduction of wind tunnel model vibration by means of a tuned damped vibration absorber installed in a model. NASA Technical Memorandum X-1606, pp 1-28, 1968.

[2] Fuykschot P. The use of friction springs for damping model vibrations. NLR STA Proceedings, National Aerospace Laboratory, 1999.

[3] Bergeron G, Dewar M, Fulchiron B, Mayaud U and Weiss J. Development of a Wind Tunnel Model Passive Vibration Damping System. *47th International Symposium of Applied Aerodynamics*, Paris, pp 1-26, 2012.

[4] Balakrishna S, Houlden H, Butler D and White R. Development of a wind tunnel active vibration reduction system. *45th AIAA Aerospace Sciences Meeting and Exhibit*, Reno, Nevada, AIAA 2007-961, pp 1-12, 2007.

[5] Chen J, Shen X, Tu F and Qureshi E. Experimental Research on an Active Sting Damper in a Low Speed Acoustic Wind Tunnel. *Shock and Vibration*, Vol. 524351, pp 1-10, 2014.

[6] Pereira J. Development of an Active Damping System for use with a Single Strut Mount. *54th AIAA Aerospace Sciences Meeting*, San Diego, California, AIAA 2016-1879, pp 1-10, 2016.

[7] McCroskey W. The phenomenon of dynamic stall. NASA Technical Memorandum 81264, pp 1-28, 1981.

[8] Le Fouest S, Depardy J and Mulleners K. The dynamics and timescales of static stall. *Journal of Fluids and Structures*, Vol. 104, 103304, 2021.